Methyl-reducing methanogenesis by a thermophilic culture of Korarchaeia

Viola Krukenberg, Anthony J Kohtz, Zackary J. Jay, Roland Hatzenpichler

Methyl-reducing methanogenesis by a thermophilic culture of Korarchaeia

Viola Krukenberg[1,*,#], Anthony J. Kohtz[1,*], Zackary J. Jay[1], Roland Hatzenpichler[1,2,#]

1, Department of Chemistry and Biochemistry, Center for Biofilm Engineering, and Thermal Biology Institute, Montana State University, Bozeman, MT-59717, USA

2, Department of Microbiology and Cell Biology, Montana State University, Bozeman, MT-59717, USA

*, These authors equally contributed to this work

#, Correspondence to viola.krukenberg@montana.edu and roland.hatzenpichler@montana.edu

Abstract

Methanogenesis mediated by archaea is the major source of methane, a strong greenhouse gas, and thus is critical for understanding Earth's climate dynamics. Recently, the genes encoding the methanogenesis pathway were discovered across multiple archaeal phyla. However, experimental verification of functional and active methanogenic pathways is currently limited to the Euryarchaeota. We here show for the first time the methanogenic capability of *Candidatus* Methanodesulfokora washburnenis, a deep-branching lineage of archaea found in hot springs that represents a novel group of methanogens in the phylum Thermoproteota. Following enrichment cultivation, we used measurements of metabolic activity and isotope tracer conversion to demonstrate methanol reduction to methane by this archaeon. Analysis of the circular genome revealed unique modifications in the energy conservation pathways linked to methanogenesis, including enzyme complexes involved in the oxidation of hydrogen or reduced sulfur compounds. The cultivation and characterization of this novel group of archaea is critical for a deeper evaluation of the diversity, physiology and biochemistry of methanogens.

Introduction

Methane is a potent greenhouse gas, and its atmospheric levels contribute to regulating Earth's climate. The majority of methane (approximately 69%) is generated in anoxic environments by methanogenic archaea[1,2] in a strictly anaerobic process called methanogenesis[3]. These microorganisms play a critical role in the global carbon cycle by catalyzing the final step in organic matter degradation and are of high interest for biotechnological applications including the production of methane as energy source[4]. Methanogens utilize compounds such as CO_2/H_2, acetate or methanol and the enzymatic pathways leading to methane formation differ depending on the substrate[3,5]. However, all methanogens employ the methyl-coenzyme M reductase (MCR) complex for the final conversion of methyl-coenzyme M and coenzyme B into methane and the CoM-S-S-CoB heterodisulfide[6]. This key enzyme also catalyzes the reversible reaction in the anaerobic oxidation of methane and other alkanes in alkanotrophic archaea[6,7]. The isolation of methanogens into axenic cultures has been fundamental to decades of research on their physiology and biochemistry[8]. To date, methanogenesis has exclusively been studied in

lineages of the Euryarchaeota, and no methanogen from outside this superphylum has ever been cultured for experimental investigation. Only recently, environmental metagenomic studies have identified genes of the methanogenesis pathway, including those in the MCR complex, to be encoded by archaea across multiple new lineages[9–15]. These newly proposed groups of methanogenic archaea could have important but so far unrecognized environmental impacts or hold undiscovered biotechnological potential.

Candidatus Methanodesulfokora washburnensis, formerly *Candidatus* Methanodesulfokores washburnensis[11,16], is a deeply branching archaeon from the phylum Thermoproteota (formerly the TACK superphylum). It was first identified as a potential methanogen by metagenome-assembled genomes (MAGs) from Washburn Hot Springs in Yellowstone National Park (YNP, WY, USA)[9,11,12]. Metabolic reconstruction predicted methyl-reducing hydrogen-dependent methanogenesis among other possible respiratory pathways, including anaerobic oxidation of methane and sulfite reduction [9,11,12]. The deeply branching phylogenetic position, together with the unique metabolic potential at the intersection of carbon and sulfur cycling[9,11,12] make this archaeon a prime candidate for culture-dependent research into the physiology, biochemistry, and metabolic versatility of methanogens.

Here, we combined selective cultivation with fluorescence microscopy, activity studies, and metagenome sequencing to demonstrate methyl-reducing methanogenesis by a thermophilic culture of this korarchaeon.

Methanogenic enrichments of Korarchaeia

We selected Washburn Hot Springs (WHS) and two hot springs in the Lower Culex Basin (LCB003 and LCB058) of YNP as source materials for cultivation. These hot springs ranged in temperature (64-77°C) and pH (6.1-6.5) and varied in the relative abundance of Korarchaeales-related 16S rRNA gene amplicons (0.4-3.6%; Fig. 1A, Extended Data Fig. 1). From each hot spring two anoxic incubations of sediment slurries were conducted at *in situ* temperature (WHS, 64ºC; LCB003, 77ºC; LCB058, 70°C) and supplied with methanol and hydrogen in the presence or absence of antibiotics. Within 64 to 67 days of incubation we detected a strong increase in the relative abundance of both 16S rRNA and *mcrA* gene amplicons identified as *Ca*. M. washburnensis. *Ca*. M. washburnensis dominated the microbial community of all six incubations, constituting up to 86% relative abundance. Other MCR-encoding archaea affiliated with Methanomethyliales, Archaeoglobales and Methanobacteriales were also detected. All incubations showed methane production (Fig. 1A), with two incubations (LCB003-1A,1B and LCB058-1B) containing near-exclusively *mcrA* gene sequences related to *Ca*. M. washburnensis (Korarchaeales, >98.5% relative abundance). The highest methane levels were observed in two incubations (WHS-B and LCB003-A), which, based on 16S rRNA gene amplicon data, were co-enriched in *Ca.* M. washburnensis and *Methanothermobacter* sp., a thermophilic, obligate CO_2-reducing hydrogenotrophic methanogen previously isolated from geothermal environments of YNP[17,18].

As inoculum for the further cultivation of *Ca*. M. washburnensis we selected one of these initial enrichments (LCB003-1B; Fig. 1A), in which methane production of up to 0.6% headspace gas

was measured. The microbial community of this culture lacked previously cultured Euryarchaeotal methanogens and was strongly dominated by *Ca*. M. washburnensis (65% and 99.9% relative abundance of 16S rRNA and *mcrA* gene amplicons, respectively). For selective cultivation, we designed a medium that matched the growth requirements for hydrogen-dependent methyl-reducing methanogenesis as predicted from metabolic reconstructions of *Ca*. M. washburnensis MAGs[9,11,12]. Methanol (10 mM) and hydrogen (50%) were supplied as methanogenic substrates, antibiotics were amended to reduce bacterial growth, and incubation was conducted at *in situ* temperature of 77°C, allowing the growth of thermophiles. Activity was monitored by measuring methane concentrations in the headspace and cultures were transferred at late exponential phase of methane production. Continuous transfers of the active methanogenic culture into fresh media resulted in a sediment-free culture, designated culture LCB3. During 13 continuous cultivation cycles (*i.e.*, transfers; over 500 days total) the final methane concentration and methane production rate increased steadily from a maximum of 2% to 5% headspace gas, equivalent to about 2 mM of methane and from approximately 63 to 38 days, respectively (Fig. 1B). Importantly, the temperature at which culture LCB3 grows is well above the known upper temperature limit for methanol-utilizing methanogens[19,20] and near the boiling point of methanol (84°C at 200 kPa), which likely reduced the amount of methanol effectively available in the liquid media.

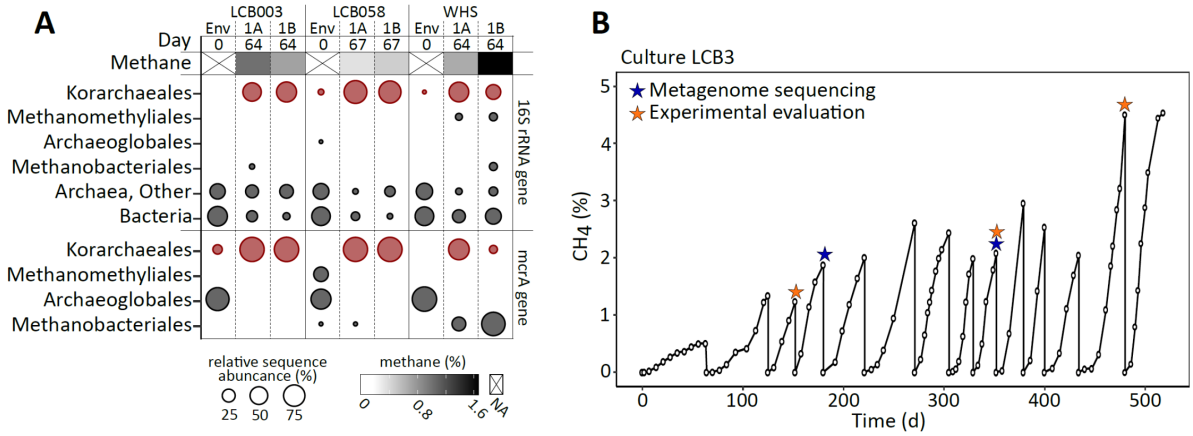

Figure 1. Methane-producing enrichment cultures from hot spring sediments. A. Relative abundance of Korarchaeales (red) in hot spring sediments (Env) and in initial enrichments (1A, 1B) after 64-67 days inferred by amplicon sequencing of *mcrA* and 16S rRNA genes. Enrichments were established from three hot springs in the Lower Culex Basin (LCB003, LCB058) and Washburn Hot Springs (WHS). Enrichments were supplied with methanol and hydrogen in the absence (1A) or presence (1B) of antibiotics. Circle sizes are proportional to relative sequence abundance (%). Lineages containing MCR-encoding archaea are depicted on order level, relative abundances >1% are shown. Shading of squares indicates methane concentrations (%) detected in the enrichment headspace. **B.** Headspace methane development during long-term cultivation. Culture LCB3 was generated from initial enrichment LCB003-1B (shown in A) and was maintained in anoxic media amended with methanol plus hydrogen and antibiotics. Stars indicate timepoints at which metagenome sequencing (blue) and experimental evaluation (orange) of culture LCB3 was performed.

Methyl-reducing methanogenesis

Fluorescence *in situ* hybridization (FISH) on culture LCB3 using a probe specific for the 16S rRNA of *Ca*. M. washburnensis revealed abundant filamentous cells (Fig. 2A, Extended Data Table 1, Fig. 2), similar in morphology to the previously described non-methanogenic *Ca.* Korarchaeum cryptofilum[21]. Filaments varied in lengths between approximately 3 µm to >20 µm, and filaments were observed both individually and in cell aggregates. We tracked the growth of *Ca*. M. washburnensis in culture LCB3 by catalyzed reporter deposition (CARD)-FISH. This showed that its relative cell abundance increased with methane production from approximately 30% during lag phase to 70% during log phase (Fig. 2A). Based on cell counts, the total cell density of culture LCB3 reached 2×10^7 cells mL^{-1} with an estimated doubling time of six days. By growing culture LCB3 in the presence of ^{13}C-methanol and measuring the transfer of isotopic label into ^{13}C-methane, we confirmed that methanol was converted to methane (Fig. 2B). Methane production ceased upon addition of bromoethanesulfonate (BES), an inhibitor of the MCR complex.

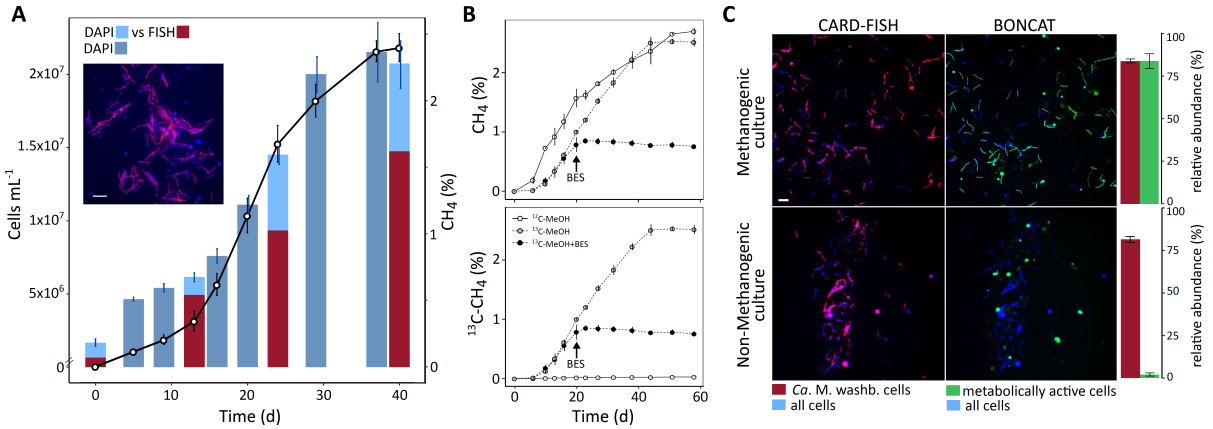

Figure 2. Physiological experiments on culture LCB3. A. Methane production and fraction of *Ca*. M. washburnensis cells. Relative abundance of *Ca*. M. washburnensis cells was determined at four time points (day 0, 12, 24, 40) based on the fraction of *Ca*. M. washburnensis specific FISH counts (red) versus total counts of DAPI stained cells (blue). Error bars indicate the standard deviation of four biological replicates. **B.** Production of ^{12}C-methane and ^{13}C-methane in cultures amended with ^{12}C-methanol (open symbols, solid line) or ^{13}C-methanol (grey symbols, dashed line). No ^{13}C enrichment of methane was detected in cultures amended with ^{12}C-methanol. BES addition to active cultures resulted in the inhibition of methanogenesis (black circles, dashed line). Error bars indicate the standard deviation of three biological replicates. **C.** Anabolic activity of cells in culture LCB3 visualized via BONCAT (green), combined with CARD-FISH (red) to identify *Ca.* M. washburnensis cells. *Ca.* M. washburnensis cells were translationally active in a methane-producing culture but not in a culture in which methanogenesis was inhibited with BES. In methanogenic cultures BONCAT-labelled cells (green bar) and CARD-FISH labelled cells (red bar) each accounted for 84% of all DAPI stained cells. In non-methanogenic cultures BONCAT-labelled cells accounted for 2% while CARD-FISH labelled cells accounted for 82%. This suggests that anabolic activity of *Ca*. M. washburnensis cells stops when methanogenesis is inhibited. Error bars indicate the standard deviation of three biological replicates. Scale bars 5 µm.

To provide evidence for methanogenesis by *Ca*. M. washburnensis, we evaluated its activity under methanogenic and non-methanogenic conditions using a combination of bioorthogonal non-canonical amino acid tagging (BONCAT) and FISH. For this, two replicate culture sets

were grown to exponential phase, at which point one set was inhibited with BES before both sets were spiked with the amino acid analog *L*-homopropargylglycine (HPG) to trace translationally active cells (Extended Data Fig. 3). We visualized cells of *Ca*. M. washburnensis via CARD-FISH and identified anabolically active cells via click chemistry mediated dye-staining. Based on cell counts, *Ca*. M. washburnensis accounted for approximately 80% of the cells in both culture sets, while BONCAT-labelling revealed cellular activity of *Ca*. M. washburnensis only under methanogenic conditions (Fig. 2C). This indicated that translational activity is dependent on the activity the MCR complex. Taken together, we present the first experimental evidence that a representative of the Korarchaeia grows by methanogenesis.

Circular genome of *Ca*. M. washburnensis

Metagenome sequencing performed on culture LCB3 at two time points (day 180 and 352, Fig. 1B) resulted in the recovery of a complete, closed chromosome that was highly related to previously obtained *Ca.* M. washburnensis MAGs (NM4, LMO9, and MDKW; Extended Data Table 2)[9,11,12]. This was apparent in both average nucleotide identity and average amino acid identity (97-98%; Extended Data Fig. 4A), phylogenomic reconstruction (Fig. 3A, Extended Data Table 3, Fig. 5A), and 16S rRNA gene identity and phylogeny (99%; Extended Data Fig. 5B). We thus designate the here described archaeon as *Ca*. M. washburnensis strain LCB3. The genome of strain LCB3 is similar in size and number of coding sequences to the MAG of *Ca.* M. washburnensis NM4 and the genome of *Ca.* K. cryptofilum OPF8, but notably smaller than the MAGs of both *Ca.* M. washburnensis MDKW and LMO9 (Extended Data Table 2). MAGs NM4, MDKW, and LMO9 were independently recovered from the same metagenome dataset of Washburn Hot Springs (WHS), but processed by different bioinformatic methods [9,11,12]. The variation in recovered MAGs from WHS together with considering the size of the genome of strain LCB3, suggests that the *Ca*. M. washburnensis population in WHS consists of several strains. Based on metagenomic read mapping to the genome of strain LCB3 we estimate its abundance in the environment of WHS, LCB003, and LCB058 between 0.1 to 2.9%, and in culture LCB3 at 62-82% (Fig. 3B, Extended Data Fig. 4B). Other community members in culture LCB3 with >1% relative sequence abundance included *Archaeoglobaceae*, *Thermofilum*, and *Fervidicoccaceae* (Fig. 3B, Extended Data Fig. 5B), and we recovered nearly complete (92-99%) genomes of all three archaea (Extended Data Table 4). Consistently, application of a general archaeal CARD-FISH probe revealed filamentous and cocci shaped cells, while no bacterial cells were observed with general bacterial probes (Fig. 3B, Extended Data Table 1, Fig. 2).

Importantly, the only *mcr* genes (*mcrABG*) identified in the metagenomes from culture LCB3 at both time points belong to the genome of strain LCB3. Phylogenetic analysis of the single copy of McrA revealed that it is highly related to previously recovered McrA from Korarchaeia MAGs and an McrA gene from a metagenome of hot spring LCB003 (Fig. 3C), the source material from which culture LCB3 was obtained. This, along with the stable isotope data and metabolic activity measurements, is strong evidence that strain LCB3 is the only methanogen in the culture.

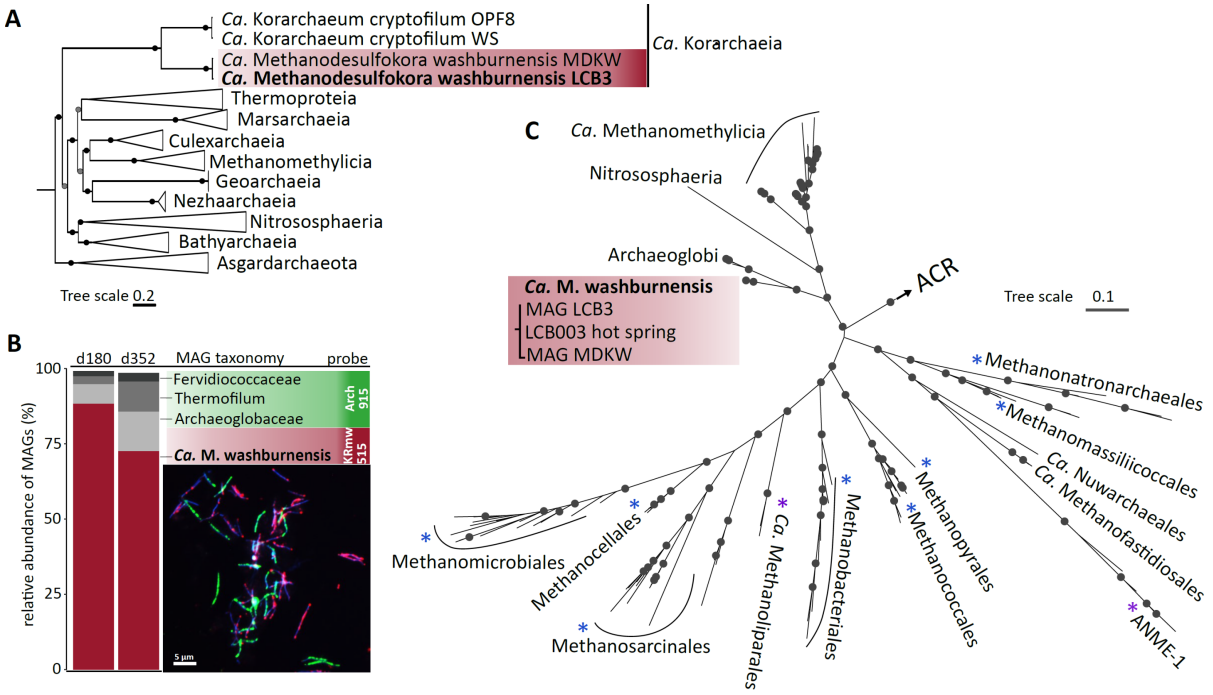

Figure 3. Phylogenetic affiliation of *Ca.* Methanodesulfokora washburnensis strain LCB3. A. Phylogenetic reconstruction based on 33 single copy marker genes showing affiliation of strain LCB3 with representative Korarchaeia genomes and MAGs. **B.** Composition of culture LCB3 based on relative abundance of recovered MAGs, and visualization of Korarchaeal (red) and other archaeal cells (green) by CARD-FISH. Note that due to two central mismatches between the 16S rRNA of *Ca.* M. washburnensis and the archaea-specific probe (Arch915, position 923 and 930), no dual labelling of *Ca.* M. washburnensis was observed. **C.** Phylogenetic tree of McrA showing the close affiliation of McrA from *Ca.* M. washburnensis strain LCB3 with McrA from MAG MDKW and McrA from the metagenome of hot spring LCB003. Asterisks indicate lineages with availability of isolates (blue) or enrichment cultures (purple), which all belong to the superphylum Euryarchaeota. Circles represent bootstrap support values >95.

Methyl-reducing methanogenesis pathway

To study the mechanisms involved in methyl-reducing methanogenesis in *Ca.* M. washburnensis strain LCB3 we analyzed its complete genome and compared it to previously described MAGs. Strain LCB3 encodes the Mcr complex (*mcrABGCD*) and methanol:coenzyme M methyltransferase (*mtaABC*) that are both required for the conversion of methanol to methane and a heterodisulfide (CoM-S-S-CoB)[3,5]. However, they lack the methyltetrahydromethanopterin:coenzyme M methyltransferase (Mtr) complex and the methyl-branch of the Wood-Ljungdahl pathway (Fig. 4, Extended Data Table 5). This supports the idea that methanogenesis in strain LCB3 is based on methyl-reduction rather than methyl-disproportionation into methane and carbon dioxide. Consequently, strain LCB3 relies on the oxidation of an electron donor, such as hydrogen, for the reduction of CoM-S-S-CoB, as previously discussed for related MAGs[9,11,12]. Importantly, all previous metabolic inferences from *Ca.* M. washburnensis MAGs suggested an energy conservation mechanism via a soluble electron-bifurcating hydrogenase/heterodisulfide reductase complex (Mvh/Hdr) coupled to a Fpo-like/HdrD complex[9,11,12]. While the LCB3 genome encodes a Fpo-like complex (Fig. 4, Extended Data Fig. 6B, Table 5) and HdrD subunits, no genes encoding an Mvh/Hdr complex were identified, which suggests an alternative route for linking hydrogen oxidation and CoM-

S-S-CoB reduction. Our metabolic reconstruction suggests that in strain LCB3 hydrogen is oxidized by a membrane-bound [NiFe]-hydrogenase of group 1g[22], and electrons are transferred via an unknown membrane-bound electron carrier to an integral membrane b-type cytochrome containing heterodisulfide reductase complex (HdrDE) that catalyzes the cytoplasmic reduction of CoM-S-S-CoB (Fig. 4, Extended Data 7B, Table 5). Different from previously characterized group 1 [NiFe]-hydrogenases of the 1k/1j type (or Vht/Vho, respectively) in methanogens, the group 1g [NiFe]-hydrogenase complex encoded in the LCB3 genome does not contain a cytochrome b subunit (Extended Data Fig. 6A). Instead, it includes two proteins with similarity to NrfC and NrfD families (Extended Data Fig. 7A). The encoded NrfD-like subunit is an integral membrane protein that could replace the function of cytochrome b in reducing a membrane-bound electron carrier[23]. Group 1g [NiFe]-hydrogenases have not been previously linked to methanogenesis and may present a unique Korarchaeia-specific differentiation in the enzymatic machinery of methanogens. Energy conservation during hydrogen-dependent methyl-reducing methanogenesis could thus rely on a simple respiratory chain of membrane-bound group 1g [NiFe]-hydrogenase and b-type cytochrome (HdrE), in which both enzyme complexes would contribute to establishing an ion gradient that subsequently can be used for the synthesis of ATP via a V-type ATP synthase (Fig. 4).

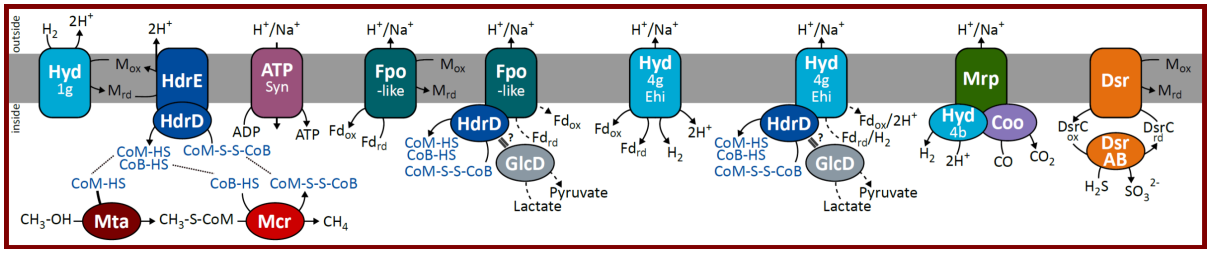

Figure 4. Metabolic reconstruction based on the genome of strain LCB3. Depicted are the methanogenesis pathway and possible alternative energy conserving complexes with linkage to methanogenesis. Abbreviations are as follows: ATP Syn, ATP Synthase; Coo, Carbon monoxide dehydrogenase; Dsr, Dissimilatory sulfite reductase; Fd, Ferredoxin; Fpo, F_{420}:Methanophenazine oxidoreductase; Glc, Lactate dehydrogenase; Hdr, Heterodisulfide reductase; Hyd, [NiFe]-Hydrogenase; Mcr, Methyl-coenzyme M reductase; Mta, Methanol:coenzyme M methyltransferase; Mrp, Na^+/H^+ antiporter; M, Membrane-bound electron carrier; ox, oxidized form; rd, reduced form. Dashed lines represent alternative reactions, dotted lines exemplify CoM-S-S-CoB recycling, color-coding differentiates proteins/protein complexes.

Alternative energy-conserving complexes

Additional enzyme complexes encoded in the LCB3 genome could facilitate either the internal production of hydrogen or allow for alternative mechanisms of energy conservation during methanogenesis. Strain LCB3 encodes a membrane-bound group 4 [NiFe]-hydrogenase also found in diverse Thermoproteota lineages affiliated with a novel cluster, termed here Ehi (Extended Data Fig. 6A, Table 5). It may function similar to the Ech or Ehb-type hydrogenases characterized in Euryarchaeotal methanogens[8], oxidizing hydrogen at the expenditure of an ion gradient to produce reduced ferredoxin[24], which could be used at a Fpo-like/HdrD complex for the reduction of CoM-S-S-CoB (Fig. 4). The reverse reaction may play a role in energy

conservation, with the oxidation of ferredoxin coupled to the production of hydrogen and ion translocation. Additionally, this Ehi hydrogenase could potentially form a complex with HdrD, allowing for coupling the direct oxidation of hydrogen to the reduction of CoM-S-S-CoB and translocation of ions across the membrane (Fig. 4), functionally similar to the HdrB-associated hydrogenases in other Thermoproteota lineages[9,25]. Strain LCB3 encodes an additional membrane-bound group 4b [NiFe]-hydrogenase/carbon monoxide dehydrogenase complex that could couple the oxidation of carbon monoxide to the production of hydrogen and translocation of ions across the membrane[26,27]. This would provide an internal source of hydrogen for methanogenesis and a means of energy conservation.

As an alternative to hydrogen, strain LCB3 also encodes the potential to use hydrogen sulfide as electron donor. The encoded cytoplasmic DsrAB complex could catalyze the oxidation of sulfide to sulfite with electron transfer via the DsrC protein to the membrane-bound b-type cytochrome containing DsrMK complex for the reduction of a membrane-bound electron carrier (Fig. 4). This would allow sulfide oxidation to be coupled to CoM-S-S-CoB reduction and energy conservation, a process not known in any other cultured methanogens. In addition, strain LCB3 as well as other MCR-encoding archaea within the Thermoproteota contains adjacent genes encoding HdrD and GlcD, which has homology to lactate dehydrogenase. This suggests that lactate could be used as an electron donor, providing electrons to HdrD for the reduction of CoM-S-S-CoB[13,14] coupled to the translocation of ions at either a Fpo-like or Ehi complex, a mechanism also not described in cultured methanogens.

In summary, the metabolic reconstruction of *Ca*. M. washburnensis strain LCB3 is consistent with methyl-reducing hydrogenotrophic methanogenesis from methanol, and indicates that the archaeon possibly uses a diverse and unique set of enzymes to conserve energy. Future work will be required to understand the interplay between carbon, hydrogen, and sulfur cycling in strain LCB3, explore alternative electron donors, and study under which conditions this archaeon might change its energy-conserving strategy entirely.

Conclusion

The cultivation of the elusive methanogen *Ca*. M. washburnensis enabled us to gain first insights into its growth and metabolism under laboratory conditions. Thermophilic cultures of strain LCB3 formed methane from methanol and cellular activity of strain LCB3 was reliant on the function of the MCR complex. This demonstrates the capacity for methanogenesis exists in the deepest branching archaeal lineage of the Thermoproteota, which may have important implications for the evolution and diversification of methanogens.

Strain LCB3 is a thermophile from a high temperature hot spring and its growth at 77°C extends the upper temperature range of both methyl-reducing and b-type cytochrome-involving methanogenesis. This may impact its niche differentiation, because cytochrome-based energy conservation is more efficient[8]; however, no such methanogen has been studied in this regard. To date, all members of the *Ca*. Methanodesulfokora genus have been detected exclusively in terrestrial geothermal systems[9,11,12,28] and may have evolved unique mechanisms to thrive in these often extreme and dynamic environments. Strain LCB3 appears to be specialized towards

utilizing methanol as substrate for methanogenesis. However, it encodes a diverse set of energy-conserving complexes and the potential to use electron donors other than hydrogen, which is rare in cultured methyl-reducing methanogens[5,20]. The capacity to exploit a diversity of electron sources, either directly or indirectly linked to methanogenesis, could provide *Ca*. M. washburnensis with an advantage in geothermal systems, where reduced compounds such as sulfide, hydrogen and carbon monoxide often co-occur[28,29]. Besides methanogenesis, *Ca*. M. washburnensis encode alternative energy-conserving pathways such as sulfite reduction and methane oxidation and the potential for a mixotrophic lifestyle[11]. Thus, methanogenesis, a process with comparatively low energy yield[8] ($CH_3OH + H_2 \rightarrow CH_4 + H_2O$, $\Delta G^0 \sim -112.5$ kJ mol^{-1}), may be used in addition to or alternatingly with other metabolisms, a trait rarely observed in Euryarchaeotal methanogens. Notably, the volatilization of methanol in high temperature environments might present a challenge to its use as a substrate, and alternative metabolisms may support the survival of strain LCB3 during periods of methanol starvation. Thus, our genomic and experimental evaluation of strain LCB3 indicates metabolic traits unique to this methanogen and suggests that many yet unresolved aspects of its physiology, biochemistry, cell biology and ecology await discovery.

To date, *Ca*. M. washburnensis, is the second member of the Korarchaeia obtained in an enrichment culture and contrasts the non-methanogenic *Ca*. K. cryptofilum[21]. The cultivation of *Ca*. M. washburnensis opens the possibility for fundamental research on the biology of this archaeon, which will both advance our current knowledge on Korarchaeia and expand our understanding of methanogenesis.

Etymology. *Methanodesulfokora*, *methanum* (Latin): methane, *de* (Latin): from, *sulfo* (Latin): sulfur, *kore* (Greek): young woman; *washburnensis* (Latin): pertaining to Washburn Hot Springs. The name implies a methane and sulfur metabolizing member of the class Korarchaeia within the phylum Thermoproteota, which metagenome-assembled genome was first obtained from Washburn Hot Springs in Yellowstone National Park[11]. The archaeon cultured in this study represents *Ca.* M. washburnensis strain LCB3.

Locality. Enriched from geothermally heated sediment of an unnamed hot spring, catalogued as feature LCB003[28], in the Lower Culex Basin of Yellowstone National Park, WY, USA.

Diagnosis. Anaerobic, thermophilic, methyl-reducing methanogen of filamentous morphology.

Online content

Any methods, additional references, Nature Research reporting summaries, source data, extended data, supplementary information, acknowledgements, details of author contributions and competing interests, as well as statements of data and code availability will be available as supplementary online information.

References

1. Saunois, M. et al. The global methane budget 2000-2017. Earth Syst Sci Data 12, 1561–1623 (2020).
2. Conrad, R. The global methane cycle: recent advances in understanding the microbial processes involved. Environ Microbiol Rep 1, 285–292 (2009).
3. Garcia, P. S., Gribaldo, S. & Borrel, G. Diversity and evolution of methane-related pathways in Archaea. Annu Rev Microbiol 76, 727–755 (2022).
4. Enzmann, F., Mayer, F., Rother, M. & Holtmann, D. Methanogens: biochemical background and biotechnological applications. AMB Express 8, 2–22 (2018).
5. Kurth, J. M., Huub, &, Op Den Camp, J. M. & Welte, C. U. Several ways one goal-methanogenesis from unconventional substrates. Appl Microbiol Biotechnol 104, 6839–6854 (2020).
6. Thauer, R. K. Methyl (Alkyl)-coenzyme M reductases: nickel F-430-containing enzymes Involved in anaerobic methane formation and in anaerobic oxidation of methane or of short chain alkanes. Biochemistry 58, 5198–5220 (2019).
7. Scheller, S., Goenrich, M., Boecher, R., Thauer, R. K. & Jaun, B. The key nickel enzyme of methanogenesis catalyses the anaerobic oxidation of methane. Nature 465, 606–608 (2010).
8. Thauer, R. K., Kaster, A. K., Seedorf, H., Buckel, W. & Hedderich, R. Methanogenic archaea: Ecologically relevant differences in energy conservation. Nature Reviews Microbiology 6, 579–591 (2008).
9. Borrel, G. et al. Wide diversity of methane and short-chain alkane metabolisms in uncultured archaea. Nat Microbiol 4, 603–613 (2019).
10. Hua, Z. S. et al. Insights into the ecological roles and evolution of methyl-coenzyme M reductase-containing hot spring Archaea. Nat Commun 10, 1–11 (2019).
11. McKay, L. J. et al. Co-occurring genomic capacity for anaerobic methane and dissimilatory sulfur metabolisms discovered in the Korarchaeota. Nat Microbiol 4, 614–622 (2019).
12. Wang, Y., Wegener, G., Hou, J., Wang, F. & Xiao, X. Expanding anaerobic alkane metabolism in the domain of Archaea. Nat Microbiol 4, 595–602 (2019).
13. Evans, P. et al. Methane metabolism in the archaeal phylum Bathyarchaeota revealed by genome-centric metagenomics. Science (1979) 350, 434–438 (2015).
14. Vanwonterghem, I. et al. Methylotrophic methanogenesis discovered in the archaeal phylum Verstraetearchaeota. Nat Microbiol 1, 1–9 (2016).
15. Seitz, K. W. et al. Asgard archaea capable of anaerobic hydrocarbon cycling. Nat Commun 10, 1–11 (2019).

16. Oren, A. & Garrity, G. M. Candidatus list no. 2. lists of names of prokaryotic candidatus taxa. Int J Syst Evol Microbiol 71, 1–20 (2021).

17. Zeikus, J. G., Ben-Bassat, A. & Hegge, P. W. Microbiology of methanogenesis in thermal, volcanic envirorunments. J Bacteriol 143, 432–440 (1980).

18. McKay, L. J., Klingelsmith, K. B., Deutschbauer, A. M., Inskeep, W. P. & Fields, M. W. Draft genome sequence of Methanothermobacter thermautotrophicus WHS, a thermophilic hydrogenotrophic methanogen from Washburn Hot Springs in Yellowstone National Park, USA. Microbiol Resour Announc 10, 1–3 (2021).

19. Cheng, L. et al. Methermicoccus shengliensis gen. nov., sp. nov., a thermophilic, methylotrophc methanogen isolated from oil-production water, and proposal of Methermicoccaceae fam. nov. Int J Syst Evol Microbiol 57, 2964–2969 (2007).

20. Sorokin, Di. Y. et al. Discovery of extremely halophilic, methyl-reducing euryarchaeal provides insights into the evolutionary origin of methanogenesis. Nat Microbiol 2, 1–11 (2017).

21. Elkins, J. G. et al. A korarchaeal genome reveals insights into the evolution of the Archaea. PNAS 105, 8102–8107 (2008).

22. Søndergaard, D., Pedersen, C. N. S. & Greening, C. HydDB: A web tool for hydrogenase classification and analysis. Sci Rep 6, 1–8 (2016).

23. Calisto, F. & Pereira, M. M. The Ion-Translocating NrfD-Like Subunit of Energy-Transducing Membrane Complexes. Front Chem 9, 1–17 (2021).

24. Kulkarni, G., Mand, T. D. & Metcalf, W. W. Energy conservation via hydrogen cycling in the methanogenic archaeon Methanosarcina barkeri. mBio 9, 1–10 (2018).

25. Kohtz, A. J., Jay, Z. J., Lynes, M. M., Krukenberg, V. & Hatzenpichler, R. Culexarchaeia, a novel archaeal class of anaerobic generalists inhabiting geothermal environments. ISME Communications 2, 1–13 (2022).

26. Schut, G. J., Lipscomb, G. L., Nguyen, D. M. N., Kelly, R. M. & Adams, M. W. W. Heterologous production of an energy-conserving carbon monoxide dehydrogenase complex in the hyperthermophile Pyrococcus furiosus. Front Microbiol 7, 1–9 (2016).

27. Kim, M. S. et al. Co-dependent H2 production by genetically engineered Thermococcus onnurineus NA1. Appl Environ Microbiol 79, 2048–2053 (2013).

28. Lynes, M. M. et al. Diversity and function of methyl-coenzyme M reductase-encoding archaea in Yellowstone hot springs revealed by metagenomics and mesocosm experiments. doi:10.1101/2022.08.18.504445.

29. Spear, J. R., Walker, J. J., McCollom, T. M., Pace, N. R. & Francisco, S. Hydrogen and bioenergetics in the Yellowstone ecosystem. PNAS 102, 2555–2560 (2005).

Methods

Chemicals

All chemicals were purchased from Sigma Aldrich unless otherwise specified.

Sample collection, enrichment, and cultivation

Hot spring sediment was retrieved from three geothermal features in Yellowstone National Park (YNP): LCB003 (44.57763, -110.78957; November 2020; 77°C; pH 6.5), LCB058 (44.57039, -110.80521; October 2020; 70°C; pH 6.1) located in the Lower Culex Basin (LCB), and WHS (44.76493, -110.43030; October 2019; 64°C; pH 6.4) located in the Washburn Hot Springs thermal area. A mixture of surface sediments (~1 cm deep) and spring water were collected into glass bottles sealed headspace-free with a butyl rubber stopper. Slurries were stored at *in situ* temperature for 24 h before transfer to room temperature for long-term storage. Initial enrichments were initiated within 24 h of material retrieval from LCB003 and LCB058 or within two years of material retrieval for WHS, and were set up in sterile serum vials (50 or 70 ml) under a $N_2/CO_2/H_2$ (90/5/5%) atmosphere. Slurries from LCB058 and WHS were diluted with anoxic media (1:10). Media was prepared as described previously[30] and contained KH_2PO_4, 0.5 g L^{-1}; $MgSO_4 \cdot 7H_2O$, 0.4 g L^{-1}; NaCl, 0.5 g L^{-1}; NH_4Cl, 0.4 g L^{-1}; $CaCl_2 \cdot 2H_2O$, 0.05 g L^{-1}; MES, 2.17 g L^{-1}; yeast extract, 0.1 g L^{-1}; and 0.002% (w/v) $(NH_4)_2Fe(SO_4)_2 \cdot 6H_2O$, 5 mM $NaHCO_3$, 1 ml L^{-1} trace element solution SL-10, 1 ml L^{-1} Selenite-Tungstate solution, 1 ml L^{-1} CCM vitamins[31], 0.0005% (w/v) resazurin, 10 ml g L^{-1} of coenzyme-M, 2 ml L^{-1} sodium dithionite, 1 mM dithiothreitol, 1 mM $Na_2S \cdot 9H_2O$, with pH adjusted to 6.5 with NaOH. Serum vials were sealed with butyl rubber stoppers and aluminum crimps before the headspace was degassed with N_2/CO_2 (90/10) for 5 minutes and set to 200 kPa. Hydrogen and methanol were added at final concentration of 50% and 10 mM, respectively. Two incubations were prepared from the slurry of each hot spring. One was amended with the bacterial antibiotics streptomycin (50 mg L^{-1}; inhibitor of protein synthesis) and vancomycin (50 mg L^{-1}; inhibitor of peptidoglycan synthesis) and one was not amended with antibiotics. Additional control incubations were supplied with only methanol or only hydrogen. Incubation was conducted at *in situ* temperatures. All stock solutions were anoxic and sterilized by filtration or autoclavation. After 64 days of incubation an initial enrichment from LCB003 was selected as inoculum for the cultivation of *Ca*. M. washburnensis, and transferred into anoxic media (10% v/v), amended with hydrogen, methanol and antibiotics. Cultivation was conducted at 77°C and cultures were maintained by regular transfer into fresh media (10% v/v).

Methane measurements

Methane concentrations were determined from subsamples of 250 µL headspace gas collected with a gas tight syringe (Hamilton) and injected into 10 mL autosampler vials sealed with grey chlorobutyl septa. Subsamples were injected into a Shimadzu 2020-GC equipped with a GS-CarbonPLOT column (30 m x 0.32 mm; 1.5 µm film thickness; Agilent) and a Rt-Q-BOND column (30 m x 0.32 mm; 1.5 µm film thickness; Restek) and operated with injector, column,

and flame ionization detector (FID) maintained at 200°C, 50°C, and 240°C, respectively. Methane concentrations were calculated based on injection of a standard curve.

Stable isotope incubation

For tracking the conversion of ^{13}C-methanol to ^{13}C-methane, active enrichment cultures were incubated in the presence of ^{13}C-methanol (99% labelled; Cambridge Isotope Laboratories). 30 ml incubations were carried out in 60 ml serum bottles with 20% (v/v) inoculum. Control incubations were performed in the presence of (i) ^{12}C-methanol (100%), (ii) ^{13}C-methanol (100%) plus bromoethanesulfonate (BES) to inhibit methanogenesis, (iii) ^{13}C-methanol (100%) plus paraformaldehyde to inhibit cellular activity, and (iv) ^{13}C-methanol (100%) without inoculum. Substrate and inhibitor were added at a concentration of 10 mM. Headspace samples were collected regularly as described above and analyzed using a Shimadzu QP2020 NX GCMS equipped with a GS-CarbonPLOT column (30 m x 0.35 mm; 30 µm film thickness; Agilent) and operated in Selected Ion Monitoring mode. The instrument was operated as described in Ai et al., 2013[32]. Peak areas corresponding to m/z ratios of 16 for ^{12}C-methane, 17 for ^{13}C-methane were used for quantification.

Fluorescence *in situ* hybridization and cell counts

Aliquots of enrichment cultures were fixed in 2% paraformaldehyde (PFA) for 1 h at room temperature, washed twice by centrifugation at 16,000xg, removing the supernatant and resuspending the cells in 1x phosphate buffered saline (PBS), before cell suspensions were stored at 4°C. For direct cell counts, aliquots of fixed cell suspensions were filtered onto polycarbonate filters (0.2 µm pore size, 25 mm diameter, GTTP Millipore, Germany) and air dried before filter pieces were cut, stained with DAPI, embedded in Citifluor-Vectashield, and enumerated under an epifluorescence microscope (Leica DM4B). Relative abundance of target cells was determined from the fraction of CARD-FISH/DOPE-FISH stained cells compared to total cell counts based on DNA stained cells using DAPI (4,6-diamidino-2-phenylindole). A 16S rRNA-targeted oligonucleotide probe (KRmw515, 5'-CCA GCC TTG CCC TCC CCT-3') specific for *Ca.* Methanodesulfokora washburnensis was designed using the probe design tool in the ARB software package[33]. Probe KRmw515 has one mismatch to the 16S rRNA of non-target organism *Ca.* Korarchaeum cryptofilum, which was absent from the culture. The horseradish peroxidase (HRP)-labelled oligonucleotide probe was synthesized by Biomers (Ulm, Germany). Stringency was tested in a catalyzed reporter deposition fluorescence *in situ* hybridization (CARD-FISH) experiment by increasing the formamide concentration in the hybridization buffer from 0% to 70%. CARD-FISH was performed as described previously[34]. Cell wall permeabilization was achieved with lysozyme treatment for 30 min at 37°C [10 mg ml^{-1} lysozyme, lyophilized powder in 0.1 M Tris–HCl, 0.05 M EDTA, pH 8] followed by proteinase K digestion for 10 min at RT [4.5 mU mL^{-1} proteinase K (Merck) in 0.1 M Tris-HCl, 0.05 M EDTA and 0.5 M NaCl, pH 8]. Endogenous peroxidases were inactivated with 0.15% H_2O_2 in methanol (30 min, RT). For hybridization, the following oligonucleotide probes were applied at their respective formamide concentration (35% for all): EUB338I-III[35], Arch915[36], NON338[37] , and KRmw515. Catalyzed reporter deposition was performed using tyramides labelled with the fluorochromes Alexa Fluor 594 or Alexa Fluor 488. When

performing double hybridizations, the peroxidase enzymes of the first hybridization were inactivated with 0.3% H_2O_2 in methanol (30 min, RT) prior to the hybridization with the second HRP-labelled probe. DOPE-FISH was performed as previously described[38]. Samples were stained with DAPI embedded in Citifluor-Vectashield, and visualized using epifluorescence microscopy.

BONCAT-FISH experiments

The metabolic activity of strain LCB3 under methanogenic versus non-methanogenic conditions was tested via biorthogonal non-canonical amino acid tagging (BONCAT). Replicate incubations of culture LCB3 were initiated with methanol and hydrogen. Inhibited controls were amended with BES at day 0. When methane production reached exponential phase (day 15), triplicate cultures were either amended with BES (5 mM) or remained unamended. After 72 h both sets were spiked with the biorthogonal amino acid HPG (100 μM). Subsamples were retrieved after 24 h, fixed in 2% PFA, washed and stored in 1xPBS at 4°C. Aliquots of fixed samples were spotted on glass slides and BONCAT-FISH was performed as previously described[39]. The fractions of BONCAT-labelled, FISH-labelled and DAPI-stained cells were enumerated to determine the relative abundance of BONCAT and FISH labelled cells.

Amplicon sequencing and analysis

DNA was extracted from environmental samples, and from initial enrichment culture (pellet from 0.5 ml) using the FastDNA Spin Kit for Soil (MP Biomedicals, Irvine, CA) following the manufacturer's guidelines. *mcrA* genes were amplified with primer set mlas-mod-F/mcrA-rev-R[40,41], and archaeal and bacterial 16S rRNA genes were amplified with the updated Earth Microbiome Project primer set 515F and 806R[42–44]. Amplicon libraries were prepared as previously described[45] and sequenced at the Molecular Research Core Facility at Idaho State University (Pocatello, ID) using an Illumina MiSeq platform with 2 x 300 bp (*mcrA* amplicon library) and 2 x 250 bp (16S rRNA amplicon library) paired end read chemistry. Both 16S rRNA and *mcrA* gene reads were processed using QIIME 2 version 2020.2[46]. Primer sequences were removed from demultiplexed reads using cutadapt[47] with error rate 0.12, reads were truncated (145 bp forward, 145 bp reverse and 260 bp forward, 200 bp reverse for 16S rRNA and *mcrA* datasets, respectively), filtered, denoised and merged in DADA2 with default settings[48]. 16S rRNA gene amplicon sequence variants (ASVs) were taxonomically classified with the sklearn method and the SILVA 132 database[49]. *mcrA* gene ASVs were assigned a taxonomy using vsearch with a minimum identity of 70% and no consensus classification against a reference database of representative near-full length *mcrA* genes encompassing the diversity of publicly available *mcrA*. Contaminants were removed using the R package decontam[50]. The *mcrA* gene dataset was curated by removing ASVs ≤400 bp and non-*mcrA* gene ASVs as identified by evaluating the top hits of a blastx search against the NCBI NR database.

Metagenome sequencing

A 50 mL aliquot of culture LCB3 was centrifuged at 16,000xg for 10 min to pellet cells, supernatant was removed, and the pellet stored at −80°C. Genomic DNA was extracted from the pellet according to Zhou et al., 1996[51], with the following modifications: (i) cells were disrupted with a tissue grinder, (ii) proteinase K treatment was extended to 1 h, and (iii) DNA was precipitated in the presence of 0.7x volumes isopropanol and 0.1x volume of 3 M sodium acetate. DNA extracts were purified using the Zymo clean and concentrator kit (DCC-10, Zymo Research) according to the manufacturer's instructions. Purified genomic DNA was used for metagenomic library construction with the Illumina DNA Prep kit following the manufacturer's recommendations and was sequenced on an Illumina NextSeq 2000 platform with 2x151 bp paired-end read chemistry performed at SeqCenter (Pittsburgh, PA).

Metagenome assembly, binning, and quality assessment

Illumina read quality, linker, and adapter trimming, artifact and common contaminate removal, and error correction were performed using the rqcfilter2 pipeline (maxns=3, maq=3) and bbcms (mincount=2, hcf=0.6) from the BBTools suite v38.94 (Bushnell B. 2014. BBMap: a fast, accurate, splice-aware aligner. https://sourceforge.net/projects/bbmap). Resulting reads were assembled with SPAdes[52] v3.15.3 (-k 33,55,77,99,127 –meta –only-assembler) and coverage was determined with bbmap (ambiguous=random). Assembled scaffolds >2000 bp were binned using Maxbin v2.2.7[53], Concoct v1.0.0[54], Metabat v2.12.1[55] (with and without coverage), and Autometa v1[56] (bacterial and archaeal modes, including the machine learning step) and bins were refined with DAS_Tool v1.1.2[57] as previously described[25]. MAG completeness and redundancy were assessed using CheckM v1.1.3[58]. The genome of strain LCB3 was determined to be circular by identifying a 127 bp sequence overlap at the start and end of the assembled contig. The overlapping sequence was removed from the end of the contig, resulting in a closed circular molecule. AAI and ANI values were computed with CompareM v0.0.23 (--fragLen 2000) (https://github.com/dparks1134/CompareM) and fastANI v1.1 (https://github.com/ParBLiSS/FastANI), respectively for available genomes and MAGs of *Ca.* M. washburnensis (n=4) and selected *Ca.* Korarchaeum (n=2) reference genomes. The closed genome of strain LCB3 was used to recruit reads from various metagenomes with bbmap (ambiguous=random) to determine the relative abundance of strain LCB3 in culture LCB3 at different timepoints and in different geothermal features of YNP.

Annotation and reconstruction of metabolic potential

The genome of strain LCB3 was annotated by the IMG/M database[59]. Catalytic subunits of [NiFe] hydrogenases (PF00374) were initially classified with HydDB and further classification was done by phylogenetic analyses[22]. Predicted optimal growth temperatures of MAGs and genomes were determined with Tome predOGT[60].

Phylogenetic analyses of marker genes

A set of 33 single-copy marker proteins were collected from Korarchaeia MAGs and reference archaeal genomes. These markers were aligned with MUSCLE[61], trimmed with trimAL[62] using

a 50% gap threshold, and concatenated to produce a final alignment of 7,118 positions. Iqtree2[63] was used to reconstruct a maximum likelihood phylogenetic tree, using the LG+F+R10 model, 1000 ultrafast bootstraps, and 1000 iterations of the SH-like approximate-likelihood ratio test[64].

16S rRNA genes from the metagenome of culture LCB3 and references were aligned and masked with ssu-align, and a maximum-likelihood phylogenetic tree was constructed with fasttree[65]. McrA from the genome of strain LCB3 and publicly available references were aligned with MAFFT-linsi[66], trimmed with trimAL[62] with 50% gap threshold and used for maximum likelihood phylogenetic analysis with Iqtree2[63] with LG+C60+F+G model and 1000 ultrafast bootstraps.

Catalytic subunits of group 1 and group 4 [NiFe]-hydrogenases were extracted from the genome, of strain LCB3 aligned against the HydDB[22] reference sequences with Mafft-LINSi[66] and trimmed with trimAL[62] using a 50% gap threshold. For group 4, additional sequences of subunits FpoD/NuoD belonging to respiratory complexes were collected from Ou et al., 2022[67] and included in the alignments. This produced final alignments of 562 and 365 residues for group 1 and group 4, respectively. Maximum likelihood phylogenetic trees were constructed using Iqtree2[63] with best fit model selected according to Bayesian information criterion and 1000 ultrafast bootstraps. The models used were LG+R10 for group 1 and LG+C60+R+F for group 4.

Reporting summary

Further information on research design is available in the Nature Portfolio Reporting Summary linked to this article.

Data availability

16S rRNA gene and *mcrA* gene amplicon data and metagenomic reads are deposited at NCBI under BioProject PRJNA913929. Metagenomes and MAGs are available on IMG/M (JGI) under IMG Genome IDs 3300005860 (WSH), 3300043541 (LCB058), 3300028675 (LCB003), 3300058130 (strain LCB3).

References

30. Laso-Pérez, R., Krukenberg, V., Musat, F. & Wegener, G. Establishing anaerobic hydrocarbon-degrading enrichment cultures of microorganisms under strictly anoxic conditions. Nat Protoc 13, 1310–1330 (2018).

31. Brandis, A. & Thauer, R. K. Growth of Desulfurovibrio species on hydrogen and sulphate as sole energy source. J Gen Microbiol 126, 249–252 (1981).

32. Ai, G., Zhu, J., Dong, X. & Sun, T. Simultaneous characterization of methane and carbon dioxide produced by cultured methanogens using gas chromatography/isotope ratio mass spectrometry and gas chromatography/mass spectrometry. Rapid Commun Mass Spectrom 27, 1935–1944 (2013).

33. Ludwig, W. et al. ARB: A software environment for sequence data. Nucleic Acids Res 32, 1363–1371 (2004).

34. Pernthaler, A., Pernthaler, J. & Amann, R. Fluorescence in situ hybridization and catalyzed reporter deposition for the identification of marine bacteria. Appl Environ Microbiol 68, 3094–3101 (2002).

35. Daims, H., Bruhl, A., Amann, R., Schleifer, K. & Wagner, M. The domain-specific probe EUB338 is insufficient for the detection of all Bacteria: Development and evaluation of a more comprehensive probe set. Syst Appl Micorbiol 22, 434–444 (1999).

36. Stahl, D. A. Development and application of nucleic acid probes. in Nucleic acid techniques in bacterial systematics 205–248 (1991).

37. Wallner, G., Amann, R. & Beisker, W. Optimizing fluorescent in situ hybridization with rRNA-targeted oligonucleotide probes for flow cytometric identification of microorganisms. Cytometry 14, 136–143 (1993).

38. Stoecker, K., Dorninger, C., Daims, H. & Wagner, M. Double labeling of oligonucleotide probes for fluorescence in situ hybridization (DOPE-FISH) improves signal intensity and increases rRNA accessibility. Appl Environ Microbiol 76, 922–926 (2010).

39. Hatzenpichler, R. et al. Visualizing in situ translational activity for identifying and sorting slow-growing archaeal− bacterial consortia. Proceedings of the National Academy of Sciences 113, 4069–4078 (2016).

40. Steinberg, L. M. & Regan, J. M. mcrA-targeted real-time quantitative PCR method to examine methanogen communities. Appl Environ Microbiol 75, 4435–4442 (2009).

41. Angel, R., Claus, P. & Conrad, R. Methanogenic archaea are globally ubiquitous in aerated soils and become active under wet anoxic conditions. ISME Journal 6, 847–862 (2012).

42. Parada, A. E., Needham, D. M. & Fuhrman, J. A. Every base matters: assessing small subunit rRNA primers for marine microbiomes with mock communities, time series and global field samples. Environ Microbiol 18, 1403–1414 (2016).

43. Apprill, A., Mcnally, S., Parsons, R. & Weber, L. Minor revision to V4 region SSU rRNA 806R gene primer greatly increases detection of SAR11 bacterioplankton. Aquatic Microbial Ecology 75, 129–137 (2015).

44. Thompson, L. R. et al. A communal catalogue reveals Earth's multiscale microbial diversity. Nature 551, 457–463 (2017).

45. Krukenberg, V., Reichart, N. J., Spietz, R. L. & Hatzenpichler, R. Microbial Community Response to Polysaccharide Amendment in Anoxic Hydrothermal Sediments of the Guaymas Basin. Front Microbiol 12, 1–11 (2021).

46. Bolyen, E. et al. Reproducible, interactive, scalable and extensible microbiome data science using QIIME 2. Nature Biotechnology 37, 852–857 (2019).

47. Martin, M. Technical Notes. http://www-huber.embl.de/users/an-.

48. Callahan, B. J. et al. DADA2: High-resolution sample inference from Illumina amplicon data. Nat Methods 13, 581–583 (2016).

49. Quast, C. et al. The SILVA ribosomal RNA gene database project: Improved data processing and web-based tools. Nucleic Acids Res 41, D590–D596 (2013).

50. Davis, N. M., Proctor, Di. M., Holmes, S. P., Relman, D. A. & Callahan, B. J. Simple statistical identification and removal of contaminant sequences in marker-gene and metagenomics data. Microbiome1 6, 1–14 (2018).

51. Zhou, J., Bruns, M. A. & Tiedje, J. M. DNA recovery from soils of diverse composition. Appl Environ Microbiol 62, 316–322 (1996).

52. Nurk, S., Meleshko, D., Korobeynikov, A. & Pevzner, P. A. MetaSPAdes: A new versatile metagenomic assembler. Genome Res 27, 824–834 (2017).

53. Wu, Y. W., Tang, Y. H., Tringe, S. G., Simmons, B. A. & Singer, S. W. MaxBin: An automated binning method to recover individual genomes from metagenomes using an expectation-maximization algorithm. Microbiome 2, 2–18 (2014).

54. Alneberg, J. et al. Binning metagenomic contigs by coverage and composition. Nat Methods 11, 1144–1146 (2014).

55. Kang, D. D. et al. MetaBAT 2: An adaptive binning algorithm for robust and efficient genome reconstruction from metagenome assemblies. PeerJ 2019, 1–13 (2019).

56. Miller, I. J. et al. Autometa: Automated extraction of microbial genomes from individual shotgun metagenomes. Nucleic Acids Res 47, 2–12 (2019).

57. Sieber, C. M. K. et al. Recovery of genomes from metagenomes via a dereplication, aggregation and scoring strategy. Nat Microbiol 3, 836–843 (2018).

58. Parks, D. H., Imelfort, M., Skennerton, C. T., Hugenholtz, P. & Tyson, G. W. CheckM: Assessing the quality of microbial genomes recovered from isolates, single cells, and metagenomes. Genome Res 25, 1043–1055 (2015).

59. Chen, I. M. A. et al. IMG/M v.5.0: An integrated data management and comparative analysis system for microbial genomes and microbiomes. Nucleic Acids Res 47, D666–D677 (2019).

60. Li, G. Rabe, K.S., Nielsen, J., Engqvist, M.K.M. Machine learning applied to predicting microorganism growth temperatures and enzyme catalytic optima. ACS Synth Biol 8, 1411–1420 (2019).

61. Edgar, R. C. MUSCLE: Multiple sequence alignment with high accuracy and high throughput. Nucleic Acids Res 32, 1792–1797 (2004).

62. Capella-Gutiérrez, S., Silla-Martínez, J. M. & Gabaldón, T. trimAl: A tool for automated alignment trimming in large-scale phylogenetic analyses. Bioinformatics 25, 1972–1973 (2009).

63. Minh, B. Q. et al. IQ-TREE 2: New Models and Efficient Methods for Phylogenetic Inference in the Genomic Era. Mol Biol Evol 37, 1530–1534 (2020).

64. Guindon, S. et al. New algorithms and methods to estimate maximum-likelihood phylogenies: Assessing the performance of PhyML 3.0. Syst Biol 59, 307–321 (2010).

65. Price, M. N., Dehal, P. S. & Arkin, A. P. Fasttree: Computing large minimum evolution trees with profiles instead of a distance matrix. Mol Biol Evol 26, 1641–1650 (2009).

66. Katoh, K. & Standley, D. M. MAFFT multiple sequence alignment software version 7: Improvements in performance and usability. Mol Biol Evol 30, 772–780 (2013).

67. Ou, Y. F. et al. Expanding the phylogenetic distribution of cytochrome b-containing methanogenic archaea sheds light on the evolution of methanogenesis. ISME Journal 16, 2373–2387 (2022).

Acknowledgements

This study was funded through a NASA Exobiology program award (80NSSC19K1633). V.K. was supported in part by a grant from the NSF (MCB-1817428). A portion of this research was performed under the Facilities Integrating Collaborations for User Science program (proposal 10.46936/fics.proj.2017.49972/6000002) and used resources at the DOE Joint Genome Institute (https://ror.org/04xm1d337), which is a DOE Office of Science User Facility operated under Contract No. DE-AC02-05CH11231. We thank the US National Park Service for permitting work in YNP under permit number YELL-SCI-8010. We thank Luke McKay and Mackenzie Lynes (both Montana State University) for discussions that informed field sampling, cultivation, taxonomy, and manuscript preparation. We thank Paige Schlegel for assistance in cultivation.

Author contributions

V.K. and R.H. developed the research project. V.K., A.J.K. and R.H. designed experiments. V.K., A.J.K. and Z.J.J. conducted field work. V.K. and A.J.K. performed cultivation. V.K. extracted DNA for amplicon sequencing and performed BONCAT and CARD-FISH experiments. A.J.K. extracted DNA for metagenome sequencing, performed FISH and stable isotope experiments, and developed GC/GCMS protocols. Z.J.J. processed and annotated metagenomic data, assembled all MAGs, analysed abundance and assigned taxonomy. A.J.K., Z.J.J. and V.K. reconstructed and interpreted the metabolic potential. Z.J.J. constructed 16S rRNA gene phylogeny. V.K. conducted phylogenetic analysis of *mcrA* and processed amplicon data. A.J.K. performed phylogenomic analysis and the classification and annotation of hydrogenases. R.H. was responsible for funding and supervision of the project. V.K. compiled the initial manuscript. All authors contributed to the writing of the final manuscript.

Competing interests

The authors declare no competing interests.

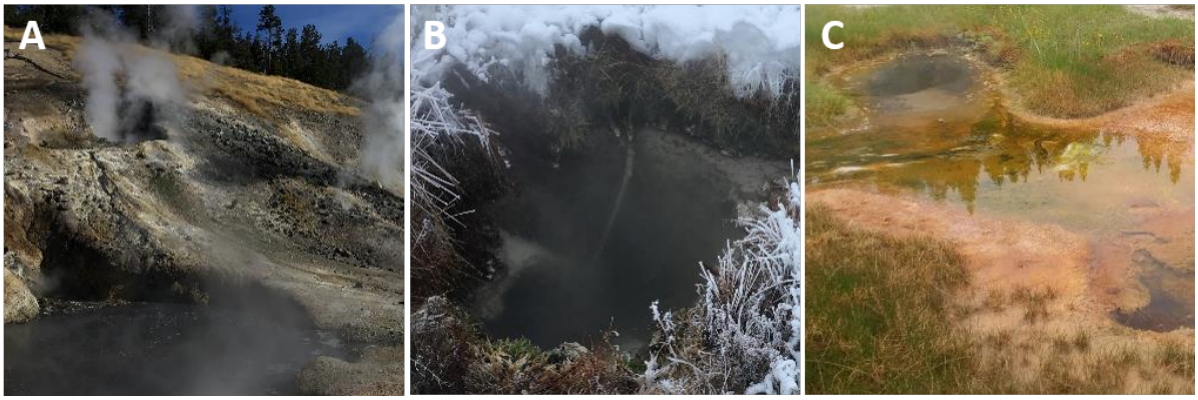

Extended Data Figure 1. Images of hot springs used as source material for cultivation. A. Washburn Hot Springs. **B**. Hot spring LCB003. **C**. Hot spring LCB058. All three hot springs are located in Yellowstone National Park (WY, USA).

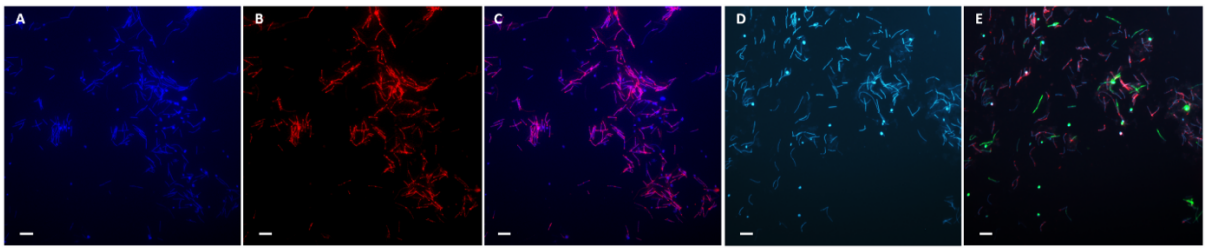

Extended Data Figure 2. Representative fluorescence micrographs of culture LCB3. A. Cells visualized with DAPI (blue). **B.** Cells visualized by DOPE-FISH using a *Ca.* M. washburnensis specific 16S rRNA-targeted oligonucleotide probe (KRmw515, red, same field of view as in A). **C.** Overlay of A and B. **D.** Cells visualized with DAPI (blue). **E.** Cells visualized with DAPI (blue, same field of view as in D) combined with dual CARD-FISH using the *Ca.* M. washburnensis specific 16S rRNA-targeted oligonucleotide probe (KRmw515, red) and a general archaea probe (Arch915, green). Note that because of two mismatches of the Arch915 probe to the 16S rRNA of *Ca*. M. washburnensis there is no overlap of signal from probes KRmw515 and Arch915. Scale bars 5 µm.

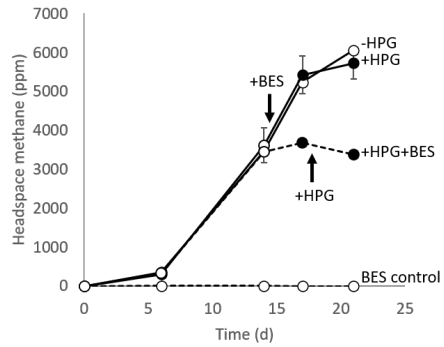

Extended Data Figure 3. Methane production in incubations for BONCAT-FISH experiments. Three replicate culture sets were grown to exponential phase. One culture set was amended with BES at day 15 (filled symbols, dashed line). At day 18 this and one additional culture set were amended with HPG (filled symbols) while another culture set was unamended (open symbols), representing growth under standard cultivation conditions. A control was amended with BES at day 0 (open symbols, dashed line) and no methane production occurred in this culture. Incubations were sampled for cell visualization via BONCAT-FISH after 24 h of incubation with HPG (day 19). Error bars indicate standard deviation from three biological replicates.

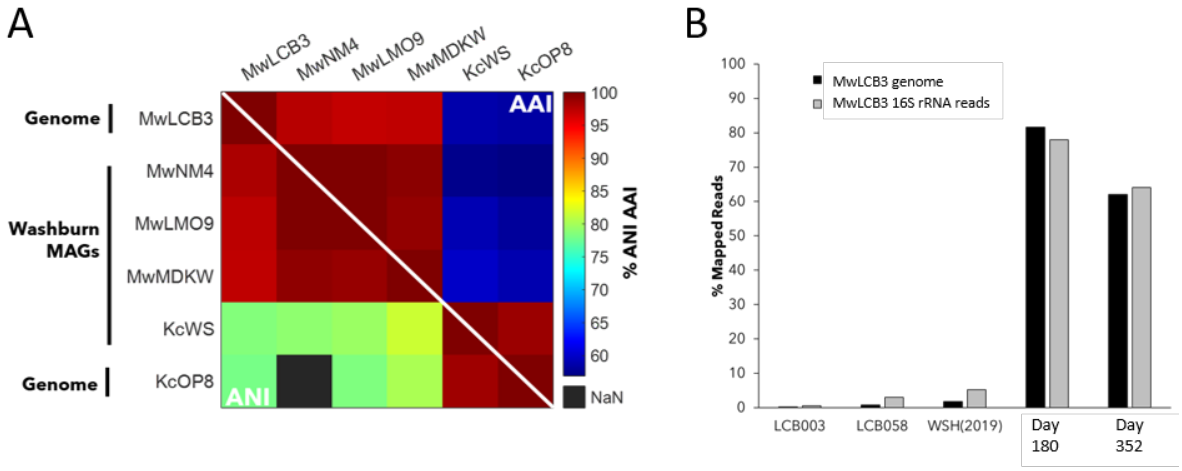

Extended Data Figure 4. Comparison of Korarchaeia genomes and MAGs. A. Pairwise comparisons of average nucleotide (below white line) and amino acid (above white line) identities (%) of *Ca*. Methanodesulfokora and *Ca*. Korarchaeum genomes and Washburn Hot Spring MAGs. **B.** *Ca*. M. washburnensis strain LCB3 genome and 16S rRNA gene read abundances in environmental metagenomes LCB003, LCB058, and WSH(2019) and culture LCB3 at day 180 and 352.

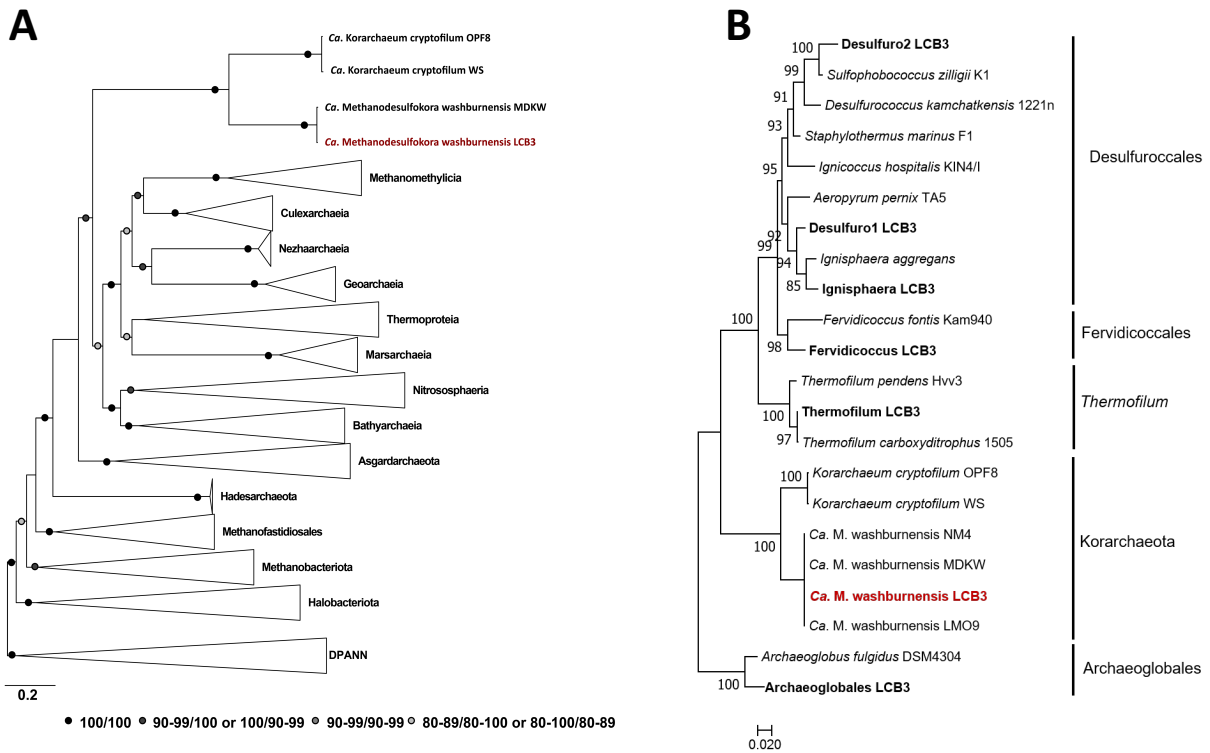

Extended Data Figure 5. Phylogenetic affiliation of *Ca*. M. washburnensis strain LCB3. A. Maximum likelihood phylogenomic tree of archaea based on 33 single copy marker genes. The tree was constructed with IQtree and the best-fit model LG+F+R10, from the concatenated alignment of conserved arCOGs. The *Ca*. M. washburnensis strain LCB3 genome is highlighted in red. Circles indicate node support via the SH-like approximate likelihood ratio and ultrafast bootstrap values, respectively. **B.** Maximum likelihood phylogenetic tree of 16S rRNA genes form culture LCB3. The tree was constructed with fasttree including the 16S rRNA gene from the LCB3 genome (red), 16S rRNA genes in MAGs from culture LCB3 and reference sequences. Bootstrap values are indicated.

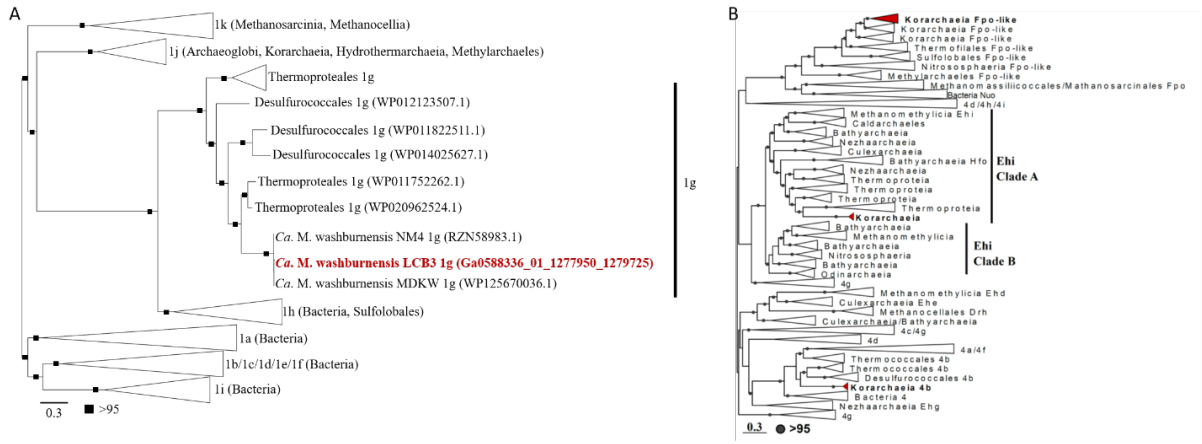

Extended Data Figure 6. Phylogenetic classification of [NiFe]-hydogenases in *Ca*. M. washburnensis strain LCB3. A. Maximum likelihood phylogenetic tree of group 1 [NiFe]-hydrogenases. The tree was constructed using IQtree2 with the best fit model LG+R10 and 1000 ultrafast bootstraps. Hydrogenase classes were assigned according to the HydDB. The sequence from the LCB3 genome is highlighted in red. Black squares indicate ultrafast bootstrap values >95. **B.** Maximum likelihood phylogenetic tree of group 4 [NiFe]-hydrogenases. The tree was constructed using IQtree2 with the best fit model LG+R10 and 1000 ultrafast bootstraps. Clades containing sequences from the LCB3 genome are highlighted in red. Black circles indicate ultrafast bootstrap values >95.

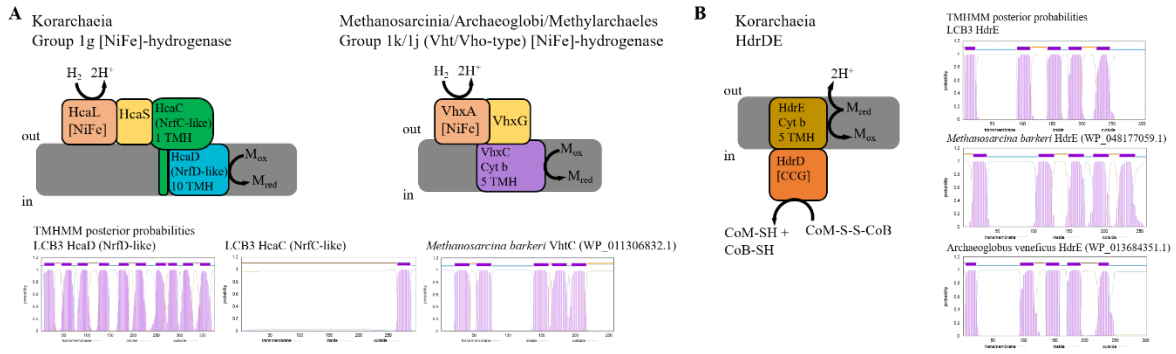

Extended Data Figure 7. Annotation of enzyme complexes in *Ca*. M. washburnensis strain LCB3. A. Comparison of group 1 [NiFe]-hydrogenase organization and structure between *Ca*. M. washburnensis strain LCB3 and other MCR-encoding archaeal lineages. Models of the enzyme arrangement in the membrane with matching colors between the models indicating conserved function. Transmembrane helix (TMH) probabilities for intermembrane subunits. Groups 1j/1k have b-type cytochrome containing subunits with five helices, while the Korarchaeia group 1g [NiFe]-hydrogenase has an NrfD-like subunit (HcaC) with ten helices and lacks b-type cytochromes. **B.** Annotation of the *Ca*. M. washburnensis strain LCB3 HdrDE complex. Model representing the arrangement of genes in the membrane. All HdrE subunits analyzed have 5 TMHs. The HdrD subunit in the LCB3 genome has cysteine residues that are conserved in HdrD subunits from other lineages. Transmembrane helices were predicted using the TMHMM 2.0 server.

Extended Data Table 1. Oligonucleotide probes used in this study.

Probe	Probe sequence (5'-3')	Specificity	Target site[1]	FA[2]	Probe label[3]	Reference
KRmw515R	CCAGCCTTGCCCTCCCCT	*Ca.* M. washburnensis	499-515	20	HRP, DOPE	This study
KR515R	CCAGCCTTACCCTCCCCT	*Ca.* K. cryptofilum	499-515	20	HRP, DOPE	Elkins et al., 2008
cKR515R[4]	CCAGCCTTACCCTCCCCT	competitor for *Ca*. K. crypto.	499-515	20	none	This study
KR565R	AGTATGCGTGGGAACCCCTC	*Ca*. K. crypto., *Ca*. M. washb.	546-565	20	HRP, DOPE	Elkins et al., 2008
Arch915	GTGCTCCCCCGCCAATTCCT	most archaea	915-935	35	HRP	Stahl&Amann, 1999
EUB338I	GCTGCCTCCCGTAGGAGT	most bacteria	338-355	35	HRP	Daims et al., 1999
EUB338II	GCAGCCACCCGTAGGTGT					
EUB338III	GCTGCCACCCGTAGGTGT					
NON338	ACTCCTACGGGAGGCAGC	negative control	338-355	35	HRP	Wallner et al., 1993

1, position in *E. coli* 16S rRNA
2, formamide concentration (v/v) in hybridization buffer
3, probe label used in this study; HRP, horseradish peroxidase; DOPE, double-labelled oligonucleotide probe
4, unlabelled competitor oligonucleotide used together with probe KRmw515 to limit probe hybridization to *Ca.* K. cryptofilum

Extended Data Table 2. Statistics of representative Korarchaeia genomes and Washburn Hot Springs metagenome assembled genomes. Seq, sequence; GC, GC content; CDS, coding sequence; pOGT, predicted optimal growth temperature; Cov, coverage; Compl, completeness; Red, redundancy; Ref, reference.

Taxon	Seq #	Length (Mb)	GC (%)	CDS	pOGT (°C)	Comp (%)	Red (%)	tRNAs	CRISPR	Ref
***Ca*. M. washburnensis LCB3**	**1**	**1.67**	**43.5**	**1,834**	**80.0**	**93.9**	**1.9**	**46**	**2**	**This study**
Ca. M. washburnensis MDKW	179	2.94	42.9	3,199	85.8	95.1	4.3	48	6	McKay et al., 2019
Ca. M. washburnensis NM4	122	1.42	43.4	1,544	80.1	85.5	1.8	44	0	Borrel et al., 2019
Ca. M. washburnensis LMO9	301	2.24	43.2	2,536	83.1	90.2	0.5	47	2	Wang et al., 2019
Ca. K. cryptofilum WS	51	1.77	48.7	1,779	76.1	95.6	3.10	47	4	McKay et al., 2019
Ca. K. cryptofilum OPF8	1	1.59	49.0	1,627	75.1	93.39	2.80	46	2	Elkins et al., 2008

Extended Data Table 3. Marker genes used in phylogenomic analysis of strain LCB3.

arCOG	Gene	Description
arCOG00785	RpmC	Ribosomal protein L29
arCOG01001	Map	Methionine aminopeptidase
arCOG01227	FtsY	Signal recognition particle GTPase
arCOG01559	FusA	Translation elongation factor G, EF-G (GTPase)
arCOG01722	RpsM/rps13p	Ribosomal protein S13
arCOG04050	FEN1	5'-3' exonuclease (including N-terminal domain of PolI)
arCOG04067	RplB	Ribosomal protein L2
arCOG04070	RplC	Ribosomal protein L3
arCOG04071	RplD	Ribosomal protein L4
arCOG04072	RplW	Ribosomal protein L23
arCOG04086	RpmD	Ribosomal protein L30
arCOG04087	RpsE	Ribosomal protein S5
arCOG04088	RplR	Ribosomal protein L18
arCOG04090	RplF/rpl6p	Ribosomal protein L6P
arCOG04091	RpsH/rps8p	Ribosomal protein S8
arCOG04092	RplE/rpl5p	Ribosomal protein L5
arCOG04094	RplX/rpl24p	Ribosomal protein L24
arCOG04095	RplN/rps14p	Ribosomal protein L14
arCOG04096	RpsQ/rps17p	Ribosomal protein S17
arCOG04097	RpsC/rps3p	Ribosomal protein S3
arCOG04098	RplV/rpl22p	Ribosomal protein L22
arCOG04099	RpsS/rps19p	Ribosomal protein S19
arCOG04169	SecY	Preprotein translocase subunit SecY
arCOG04223	SUI1	Translation initiation factor 1 (eIF-1/SUI1)
arCOG04239	RpsD/rps4p	Ribosomal protein S4 or related protein
arCOG04240	RpsK/rps11p	Ribosomal protein S11
arCOG04241	RpoA/Rpo1/rpoD	DNA-directed RNA polymerase subunit D
arCOG04242	RplM/rpl13p	Ribosomal protein L13
arCOG04243	RpsI/rps9p	Ribosomal protein S9
arCOG04245	RpsB/rps2p	Ribosomal protein S2
arCOG04254	RpsG/rps7p	Ribosomal protein S7
arCOG04288	RplJ	Ribosomal protein L10
arCOG04289	RplA/rpl1p	Ribosomal protein L1

Extended Data Table 4. Statistics of other MAGs recovered from culture LCB3. Seq, sequence; GC, GC content; CDS, coding sequence; pOGT, predicted optimal growth temperature; Cov, coverage; Comp, completeness; Red, redundancy; Abd, relative abundance.

Taxon	Seq #	Length (Mb)	GC (%)	CDS	pOGT (°C)	Comp (%)	Red (%)	tRNAs	CRISPR	Abd (%)
Archaeoglobaceae	84	1.65	43.3	1,771	75.8	99.3	0	50	2	13.2
Thermofilum	130	2.09	47.3	2,220	80.4	92.7	6.2	24	15	10.0
Fervidicoccaceae	7	1.35	44.2	1,422	92.0	96.9	3.2	33	2	2.75
Ignisphaera	233	1.72	39.9	1,708	85.2	81.9	0.6	29	1	0.75
Desulfurococcaceae	75	1.49	40.9	1,552	84.8	94.6	1.0	30	0	0.73

Extended Data Table 5. Overview of genes identified in the LCB3 genome. Included are genes discussed in the text. Locus tags refer to IMG Genome ID 3300058130 (strain LCB3).

Locus tag	Gene	Annotation
Ga0588336_01_1498205_1498459	*mcrA*	methyl-coenzyme M reductase alpha subunit
Ga0588336_01_1214849_1216177	*mcrB*	methyl-coenzyme M reductase beta subunit
Ga0588336_01_1217207_1217998	*mcrG*	methyl-coenzyme M reductase gamma subunit
Ga0588336_01_1216569_1217210	*mcrC*	methyl-coenzyme M reductase subunit C
Ga0588336_01_1216180_1216572	*mcrD*	methyl-coenzyme M reductase subunit D
Ga0588336_01_1196565_1197617	*mtaA*	methanol:coenzyme M methyltransferase
Ga0588336_01_1209784_1210245	*mtaA*	methanol:coenzyme M methyltransferase
Ga0588336_01_1208435_1209439	*mtaA*	methanol:coenzyme M methyltransferase
Ga0588336_01_1256403_1257407	*mtaA*	methanol:coenzyme M methyltransferase
Ga0588336_01_1200192_1201577	*mtaB*	methanol-5-hydroxybenzimidazolylcobamide comethyltransferase
Ga0588336_01_1201574_1202422	*mtaC*	methanol corrinoid protein
Ga0588336_01_920467_920844	*fpoA*-like	F_{420}-H_2 dehydrogenase subunit A
Ga0588336_01_919958_920482	*fpoB*-like	F_{420}-H_2 dehydrogenase subunit B
Ga0588336_01_919495_919971	*fpoC*-like	F_{420}-H_2 dehydrogenasesubunit C
Ga0588336_01_918336_919505	*fpoD*-like	F_{420}-H_2 dehydrogenase subunit D
Ga0588336_01_917317_918336	*fpoH*-like	F_{420}-H_2 dehydrogenase subunit H
Ga0588336_01_916845_917336	*fpoI*-like	F_{420}-H_2 dehydrogenase subunit I
Ga0588336_01_916379_916861	*fpoJ*-like	F_{420}-H_2 dehydrogenase subunit J
Ga0588336_01_916071_916376	*fpoK*-like	F_{420}-H_2 dehydrogenase subunit K
Ga0588336_01_912465_914540	*fpoL*-like	F_{420}-H_2 dehydrogenase subunit L
Ga0588336_01_914546_916066	*fpoM*-like	F_{420}-H_2 dehydrogenase subunit M
Ga0588336_01_911068_912468	*fpoN*-like	F_{420}-H_2 dehydrogenase subunit N
Ga0588336_01_302773_304227	*mrpA*/*mnhA*	multicomponent Na^+:H^+ antiporter subunit A
Ga0588336_01_297950_299314	*mrpD*/*mnhD*	multicomponent Na^+:H^+ antiporter subunit D
Ga0588336_01_300872_302779	*mrpD*/*mnhD*	multicomponent Na^+:H^+ antiporter subunit D
Ga0588336_01_812845_814626	*atpA*	V/A-type H^+-transporting ATPase subunit A
Ga0588336_01_809780_812845	*atpB*	V/A-type H^+-transporting ATPase subunit B
Ga0588336_01_808152_809162	*atpC*	V/A-type H^+-transporting ATPase subunit C
Ga0588336_01_809163_809780	*atpD*	V/A-type H^+-transporting ATPase subunit D
Ga0588336_01_814627_815247	*atpE*	V/A-type H^+-transporting ATPase subunit E
Ga0588336_01_815540_815872	*atpF*	V/A-type H^+-transporting ATPase subunit F
Ga0588336_01_815240_815530	*atpH*	V/A-type H^+-transporting ATPase subunit G/H
Ga0588336_01_805172_807541	*atpI*	V/A-type H^+-transporting ATPase subunit I
Ga0588336_01_807605_807925	*atpK*	V/A-type H^+-transporting ATPase subunit K
Ga0588336_01_1251631_1252734	*hdrD*	heterodisulfide reductase subunit D
Ga0588336_01_1221513_1222643	*hdrD*	heterodisulfide reductase subunit D
Ga0588336_01_1617244_1618869	*hdrD*	heterodisulfide reductase subunit D
Ga0588336_01_1618856_1619773	*hdrE*	heterodisulfide reductase subunit E, cytochrome-b
Ga0588336_01_1220248_1221516	*glcD*	putative lactate dehydrogenase
Ga0588336_01_307153_307767	*cooF*	anaerobic carbon-monoxide dehydrogenase iron sulfur subunit
Ga0588336_01_305228_307153	*cooS*	anaerobic carbon-monoxide dehydrogenase catalytic subunit
Ga0588336_01_1313931_1315136	*dsrA*	sulfite reductase subunit A
Ga0588336_01_1315152_1316216	*dsrB*	sulfite reductase subunit B
Ga0588336_01_1308276_1308596	*dsrC*	sulfite reductase subunit C
Ga0588336_01_1311720_1313183	*dsrK*	sulfite reductase subunit K
Ga0588336_01_1310918_1311718	*dsrM*	sulfite reductase subunit M
Ga0588336_01_1277950_1279725	*hyd* 1g	group 1g [NiFe] hydrogenase, catalytic subunit
Ga0588336_01_296409_297953	*hyd* 4b	group 4b [NiFe] hydrogenase, catalytic subunit
Ga0588336_01_160718_161899	*hyd* 4g Ehi	group 4g [NiFe] hydrogenase, catalytic subunit